Target Localization and Autonomous Navigation Using Wireless Sensor Networks—A Pseudogradient Algorithm Approach

Nikhil Deshpande, *Student Member, IEEE*, Edward Grant, *Senior Member, IEEE*, and Thomas C. Henderson, *Fellow, IEEE*

***Abstract*—Autonomous mobile robots (AMRs) operating in unknown environments face twin challenges: 1) localization and 2) efficient directed navigation. This paper describes a two-tiered approach to solving these challenges: 1) by developing novel wireless-sensor-network (WSN)-based localization methods and 2) by using WSN–AMR interaction for navigation. The goal is to have an AMR travel from any point within a WSN-covered region to an identified target location without the aid of global sensing and position information. In this research, the target is reached as follows: 1) by producing a magnitude distribution within the WSN region that has a target-directed pseudogradient (PG) and 2) by having the WSN efficiently navigate the AMRs using the PG. This approach utilizes only the topology of the network and the received signal strength (RSS) among the sensor nodes to create the PG. This research shows that, even in the absence of global positioning information, AMRs can successfully navigate toward a target location using only the RSS in their local neighborhood to compute an optimal path. The utility of the proposed scheme is proved through extensive simulation and hardware experiments.**

***Index Terms*—Goal-directed navigation, pseudo topological gradient, wireless received signal strength (RSS), wireless-sensor-network (WSN)-assisted target localization.**

I. Introduction

AUTONOMOUS mobile robotics systems operating in unknown and unstructured environments face fundamental challenges as follows: 1) localizing events within the region and 2) navigating autonomous mobile robots (AMRs) to identified locations in an efficient manner. These target locations can be emergent, such as fires, chemical leaks, accidents, natural disasters, and search-and-rescue operations, or preplanned, such as area explorations, agricultural operations, and robotic area cleaning. In either scenario, environmentally embedded wireless sensor networks (WSNs) can provide distributed intelligence and information richness [1]. For environmental monitoring applications, WSNs present advantages because of the following: 1) low cost; 2) low energy; 3) multifunctionality; 4) robustness; and 5) scalability. Their multifunction capability allows them to be randomly distributed and in large numbers. The diverse range of sensors that can be used with WSNs, e.g., seismic, magnetic, thermal, and visual, can provide a wealth of information regarding the state of the environment that they are monitoring [1]. In certain applications, e.g., searching for land mines and disaster relief operations, it is considered appropriate to use autonomous agents along with the WSN. Commonly, it is AMRs, with their inherent intelligence and autonomous behavior, that provide a cooperative interaction with the distributed static WSN [12]–[14], [19]. Such interactive WSN–AMR coordination poses interesting challenges in itself, including the need for the following: 1) the development of localization algorithms; 2) the provision of time-critical response capabilities; and 3) the development of efficient and distributed WSN–AMR interaction mechanisms.

Of particular interest here is efficient WSN–AMR interaction, such that the coordination between the distributed WSNs and AMRs can be optimized.[1]

A. Problem Formulation

The goal of this research is to provide the:

> "efficient navigation of AMRs to localized targets using only RSS in statically deployed WSNs in unknown environments."

In this system, wireless sensors are randomly deployed to cover an unspecified geographical area, such that they form a connected network. When any wireless sensor detects a target, each wireless sensor node gets a magnitude assigned to it. This magnitude is a function of the node's communication distance from an identified target location. As a consequence, the sensor node closest to the target (*target node*) has the highest magnitude assigned to it. A "*pseudogradient*" (PG) is created in the region, one that AMRs placed into this environment can follow to reach the target from any location within the region. Fig. 1(a) illustrates the concept. Since global positioning information is not available, it is only the wireless received signal strength (RSS) that is used to generate the PG. Using RSS to assign the node magnitudes has proved to be advantageous in such unknown environments, because it is a low-complexity approach; RSS can also give a good indication of noise and obstacle presence in the environment [17].

Manuscript received April 22, 2011; revised November 6, 2012 and December 22, 2012; accepted January 17, 2013. Date of publication August 15, 2013; date of current version February 5, 2014.

N. Deshpande and E. Grant are with the Department of Electrical and Computer Engineering, North Carolina State University, Raleigh, NC 27695 USA (e-mail: nadeshpa@ncsu.edu; egrant@ncsu.edu).

T. C. Henderson is with the School of Computing, University of Utah, Salt Lake City, UT 84112 USA (e-mail: tch@cs.utah.edu).

Color versions of one or more of the figures in this paper are available online at http://ieeexplore.ieee.org.

Digital Object Identifier 10.1109/JSYST.2013.2260631

[1]This paper is an expansion of the research published in [9].

1932-8184 © 2013 IEEE. Personal use is permitted, but republication/redistribution requires IEEE permission.
See http://www.ieee.org/publications_standards/publications/rights/index.html for more information.

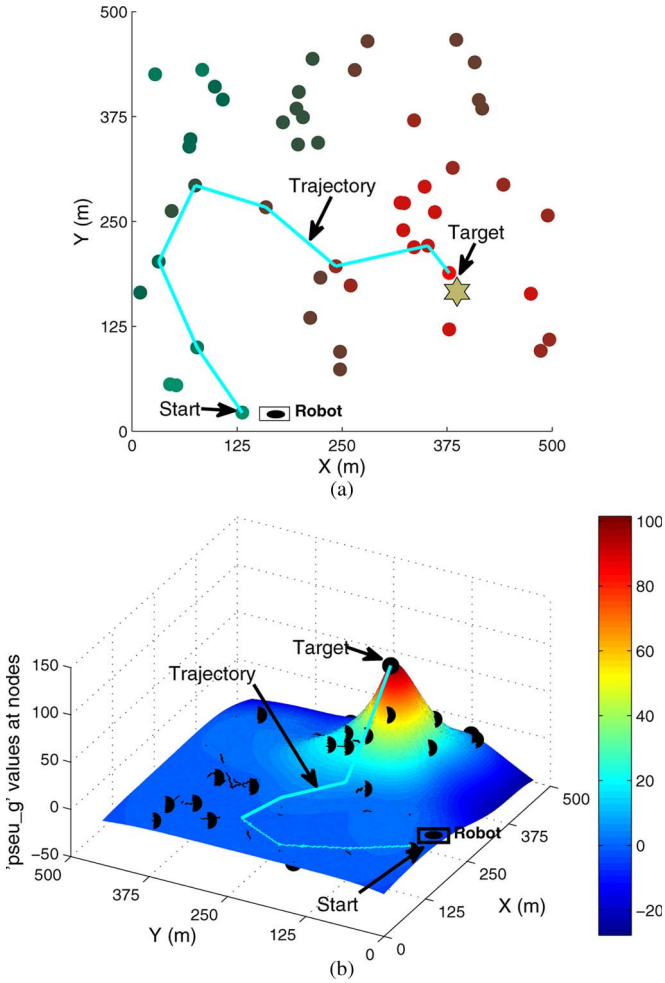

Fig. 1. PG in a region using PG algorithm. (a) Magnitude distribution in the WSN. (b) Interpolated image depicting the function magnitude distribution.

B. Contributions

Novel techniques for target localization and WSN-guided AMR navigation are introduced in this paper, including the following: 1) providing a distributed target localization algorithm that generates a navigable path for AMRs in the WSN-covered region, an algorithm that uses wireless RSS information only; 2) providing a localized WSN–AMR interaction algorithm that navigates the AMRs by estimating the PG at each sensor node location; and 3) providing performance metrics which compare the implementations of these algorithms in the simulated and real worlds.

The remainder of this paper is organized as follows. Section II discusses related work in this area. Section III introduces the algorithm and discusses its applicability, while Section IV introduces the WSN-assisted navigation protocol. Section V discusses the implementation of the algorithm with experimental results. Section VI summarizes this paper with a note on future work.

II. Previous Work

The research in this paper was inspired by the research into WSNs and AMR navigation in [3], [7], [12]–[14], and [19]. Basically, there are two research themes in the field; these are centered on the development of the following: 1) position-aware algorithms and 2) position-unaware algorithms. Position-aware schemes require a global positioning capability for WSN nodes, like GPS or a prior implemented localization scheme. Conversely, position-unaware schemes require algorithms that are independent of the locations of the nodes. They utilize the present topology of the WSN and base their control strategies on the immediate neighborhood of the nodes. The algorithms in this paper are in the position-unaware category.

A. Position-Aware Approaches

Li *et al.* [14] show WSNs using artificial potential fields to navigate AMRs to a goal location keeping as far away from "dangerous" (obstacle) sites as possible. In [11], Henderson and Grant present three algorithms for a gradient-following technique for an AMR to reach a detected target. The inherent gradient present in the phenomenon being sensed is utilized for the purpose. Kotay *et al.* [13] explore the use of synergy between GPS-enabled AMRs and networked sensors to provide localization, path planning, and improved navigation. In [24], Verma *et al.* propose a scheme assuming the availability of a positioning device to guide the mobile sensor nodes to a goal, assisted by a WSN, with artificial potential field methods. In [4] and [26], the authors discuss how WSNs are used to mediate AMR task allocations and algorithms for optimized sensor deployment. Arora *et al.* [2] present an exhaustive theoretical and experimental analysis of a distributed sensing architecture for target detection, classification, and tracking. Finally, Severino and Alves [20] demonstrate a centralized scheme where a control station, using the distance information to a target and known anchor nodes, estimates the location of the target using a min–max-based localization algorithm.

As is seen, all these methods require some technological ability to ascertain their position in a global frame (e.g., GPS and magnetic compass).

B. Position-Unaware Approaches

Chen and Henderson [7], the early proponents of the "smart" WSN as an "information field," use a model for temperature dissipation in a region to estimate internode distances and assist multiple AMR coordination. In [3], Bachrach *et al.* present a scheme using the following: 1) communication hops (and RSS) of nodes from only one known node location to estimate distances and 2) iterative gradient descent to arrive at the (x, y) node positions. In [8], Corke *et al.* describe a scheme using a flying robot to perform the following: 1) to localize sensor nodes and ii) to navigate AMRs and humans through the region using localized nodes. Sheu *et al.* [21] propose a scheme where the direction of motion of the AMR is based on to-and-fro movement of the AMR itself. This implementation is vulnerable to the environmental variation in RSS values as well as not being quick and efficient with all the back-and-forth movements. In [5], Batalin *et al.* describe a value-iteration-based method where the AMR uses preassigned transition probabilities between sensor nodes to maximize its probability of reaching a target. Luthy *et al.* [15] discuss the coordination of AMRs in repairing disconnected WSNs, based on RSS. The variability and interference issues in RSS are presented through several

hardware experiments. Reich and Sklar [19] propose a scheme using communication hop-count-based gradients for AMR navigation. The implementation does not account for proximity/distance of nodes to targets or to each other, nor the RSS values. Jiang *et al.* [12] present a scheme introducing the following: 1) an RSS-based farthest-node-forwarding (FNF) broadcast method and 2) a tree-assisted AMR navigation scheme. The authors show improved performance in time and energy efficiency of the WSN–AMR coordination.

III. Distributed Algorithm for Target Localization

Fig. 1(a) is also a depiction of the PG distribution in the form of a color dispersion in an AMR navigation region of interest. The *target node* is "dark red," and the color fades to "blue" away from the *target node*. It is up to the PG algorithm to present a directed path from start-to-end to the AMR. In effect, the complexity and burden of motion planning are now shared by the AMR and the distributed intelligence inherent in the WSN.

Two important characteristics of WSN-based systems are as follows: 1) RSS and 2) communication hop count.

1) The RSS gives an indication of the intensity of the signal in a wireless communication link [10]. It provides a metric for assessing how stable a connection is given environmental changes, e.g., noise, obstacles, and interference. For instance, if an RSS value is -70 dBm, then the communication channel will result in better quality of link between the transmitter and receiver than when the RSS value is -90 dBm. On the other hand, if ideal environmental conditions are assumed, then the same reduction in RSS is an indication of increasing distance between the transmitter and the receiver. Signal strength versus distance estimates have been empirically analyzed in [6] and [25].
2) Hop count gives an indication of the Euclidean distance of a particular node in a WSN from a source node that initiates a flooding message. This value is dependent on the communication range of the nodes as well as the physical distance of the nodes themselves. This concept essentially derives from the breadth-first search tree [23], where each node maintains a minimal hop count to the source node.

A. Sensor/AMR Model

The locations of the sensor nodes are assumed to be drawn from a uniform random distribution over a 2-D planar region. It is assumed that the WSN is connected, i.e., there exists a communication path (of any length) from every node to every other node in the WSN [23].

Each node in the WSN has a unique identification (ID) and consists of a processing unit, memory, radio, power source, and one or more sensors of different types. Factors such as size, cost, and lifetime constrain the sensor nodes in their memory and energy consumption. The communication range of these nodes is also limited such that the entire network cannot be traversed in a single communication hop. Every WSN node has a variety of sensors attached to it, including thermal, chemical, accelerometer, pressure, humidity, etc.

The PG algorithm is initiated by a *target node*. With the absence of a global reference frame, a sensor node that can sense a target cannot determine how many other sensors can sense the same target, except its neighbors. It is assumed that the sensors can estimate an intensity of the sensed target at their locations. This intensity can be used to indicate the distance of the sensed event from the sensor. Then, whether a sensor node identifies itself as the *target node* is inversely proportional to this estimated distance. Using a simple back-off-before-transmission algorithm, the neighborhood of the node closest to the target resolves the identity of the *target node*. Relatedly, having multiple *target nodes* can also be advantageous since it can allow AMRs with multiple approach directions to a target. This artifact is explored in a separate paper.

The AMR is equipped with wheels for locomotion along with computing capabilities. It has the capability to communicate with the WSN—it uses directional antennas for bearing estimation and an omnidirectional antenna for RSS-based ranging.

B. Algorithm

The PG algorithm requires each sensor to calculate a magnitude. The magnitude depends on its communication distance from the target itself, which, in turn, utilizes the communication hop count and the RSS in the node neighborhood. Each sensor node implements the algorithm (Algorithm 1) independently by interacting with its immediate neighborhood. The algorithm utilizes the best total RSS estimate to a particular *target node* to calculate the magnitude at each node. In essence, every node senses its vicinity for a particular target. The node closest to the target marks itself as a *target node* and initiates a packet exchange via the flooding mechanism. This allows subsequent nodes to set their hop count as well as a magnitude, denoted by "$pseu\_g$." The *target node* sets its own magnitude as the highest in the region (this value is available to all the nodes as a preset). The hop count for the *target node* is set as zero.

Algorithm 1 PG Magnitude Distribution Algorithm

1: Set MAX_PG; Hop Count $=$ MAX_HC;
2: **if** target $=$ nearby **then** node $=$ target node
3: Hop Count $= 0$;
4: $pseu\_g =$ MAX_PG;
5: broadcast [$pseu\_g$; Hop Count];
6: **else** ▷ node is not *target node*
7: Get RSS_i, Hop Count$_i$, $pseu\_g_i$ from neighbor i
8: Calculate $pseu\_g_i^{\text{calc}}$ from

$$pseu\_g_i^{\text{calc}} = pseu\_g_i \bullet (\text{RSS}_i) \tag{1}$$

9: Hop Count$_i^{\text{calc}}$ $=$ Hop Count$_i + 1$;
10: **if** (Hop Count$_i^{\text{calc}} \leq$ Hop Count) && ($pseu\_g_i^{\text{calc}} > pseu\_g$) **then**
11: Store Hop Count $=$ Hop Count$_i$;
12: Store $pseu\_g_i^{\text{calc}}$ as $pseu\_g$;
13: broadcast [$pseu\_g$; Hop Count];
14: **end if**
15: **end if**

As shown in the algorithm, the calculated value of $pseu\_g$ at a node scales the received $pseu\_g_i$ value from the neighbors by their respective RSS values. Logarithmic values of RSS are used here, and since the dBm values of RSS are negative [10], they are scaled to the interval [0, 1], based on the maximum and minimum sensitivity settings of the TMote Sky nodes [16]. A key aspect of the algorithm is that the sensor node retains the highest $pseu\_g$ value after getting updates from its neighbors. Therefore, every node only broadcasts its highest $pseu\_g$ value to its neighbors, avoiding retransmission of any redundant messages.

For a 50-node WSN, the black dots in Fig. 1(b) represent the node locations with their elevation representing the magnitudes. As seen, the global maximum exists close to the actual target location (the highest node is the *target node*). The magnitude then decreases away from the target.

C. Analysis of Algorithm

This section presents the theoretical analysis for the PG algorithm. For the purposes of analysis, the only assumption made is that the network is a connected graph. This assumption implies that, even if the environmental conditions are nonideal, i.e., noise, obstacles, node or link failures, etc., every node in the network has at least one neighbor node within active communication range.

1) Hop-Distance Model: It is noted from the algorithm that the *target node* initiates the flood, after setting its hop count to zero. Each subsequent sensor node increments the hop-count value that it receives by one, before broadcasting the message to its neighbors. In this way, every sensor node maintains a minimum hop count to a *target node*. This minimum hop count becomes the length of the path from a node to the *target node* in terms of communication distance. Since a constant communication radius of r is assumed, a sensor node with a hop count of h would be at most a distance of $h * r$ from the *target node*.

Theorem 1: There is no local maximum in the $pseu\_g$ magnitude distribution in the WSN, except at the *target node*.

a) Proof: As shown in Algorithm 1, the *target node* has the MAX_PG value. For a connected network, the *hop-distance model* implies that each node will have a neighborhood with at least one lower hop-count neighbor. (Ideally, each node has neighbors with hop counts one higher than, equal to, and one lower than itself [3].) The only exception would be the *target node* having all neighbors with a higher hop count. A local maximum in this scheme would imply that a node has a higher $pseu\_g$ value than all its neighbors. As per Algorithm 1 and (1), this implies that this node has a lower hop count than all its neighbors. The only node that satisfies this condition is the *target node* itself. This means that the maximum is global, not local. In other words, any node other than the *target node* in the network would have a positive gradient at its location, navigating the AMR toward the *target node*. ■

Theorem 2: If a node has a $pseu\_g$ value, then there exists a path from that node to any target located in the region covered by the WSN.

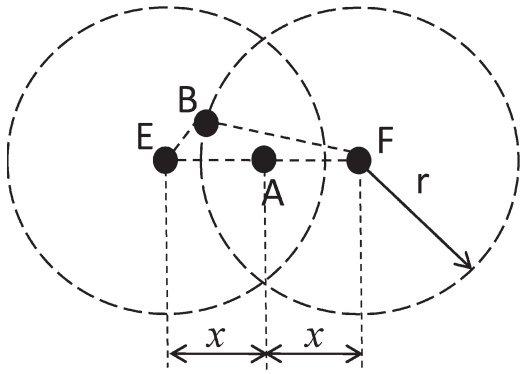

Fig. 2. *Target-node* neighborhood for PG algorithm.

b) Proof: Since the network is a connected graph, if a node has a $pseu\_g$ value, then it indicates that the node has a neighborhood with at least one other node. Following Theorem 1, there exists a positive PG at this node. Thus, the node has a path leading toward the *target node*. Consequently, a connected graph implies that this node would have a path to any target within the coverage area of the WSN. ■

2) Preferred Navigation Path: The following analysis illustrates how the distribution of $pseu\_g$ values impacts the choice of the navigation path for the AMR.

The PG algorithm assigns $pseu\_g$ values at a node by scaling the received $pseu\_g$ value from its neighbors by the RSS value of the message. Assuming an ideal environment, the RSS value decreases with increasing distance. It is known that the RSS–distance relationship is nonlinear. In the absence of any knowledge of the environment and the atmospheric conditions of a deployed region, it is generally assumed that RSS varies as the inverse square of distance [10].

In Fig. 2, node E is a *target node*, and node A lies on the straight-line path between nodes E and F. All nodes are assumed to have the same communication radius r values (the *dotted lines* indicate r). Assume that the node arrangement in Fig. 2 is such that $d_{EB} = x/2$. The corresponding RSS values are RSS_{EA}, RSS_{EB}, RSS_{EC}, and so on. Without loss of generality, the RSS values are calculated using the following equation [10]:

$$\mathrm{RSS} = \frac{\gamma}{(\mathrm{distance})^2} \tag{2}$$

where γ is a constant. From triangle inequality, it is noted that $d_{EA} + d_{AF} < d_{EB} + d_{BF}$. Therefore, the distance estimate for node F is the lowest for a message from node A. For a general location of node B, $\angle BEA$ can have any value in the interval $(0, \pi/3)$. Then, $\angle EFB$ varies in the interval $(0, \pi/3)$. For purposes of analysis, it is assumed that $\angle BEA = \pi/4$. Then, $d_{BF} = 1.684 \cdot x$.

The $pseu\_g$ value of node E is MAX_PG (from Algorithm 1). It is noted from Algorithm 1 that nodes A and B have a hop count of one and node F has a hop count of two. Considering these locations, the calculated $pseu\_g$ values[2] at each node using (1) are shown in Table I.

[2]The $pseu\_g_x^y$ notation is read as $pseu\_g$ value [19] at node y due to message from node x.

TABLE I
pseu_g VALUES AT EACH NODE

Node Pair	*pseu_g*-value	Node Pair	*pseu_g*-value
$pseu\_g_E^A$	$\frac{MAX\_PG}{x^2}$	$pseu\_g_A^F$	$\frac{MAX\_PG}{x^2} \cdot \frac{1}{x^2}$
$pseu\_g_E^B$	$\frac{4 \cdot MAX\_PG}{x^2}$	$pseu\_g_B^F$	$\frac{4 \cdot MAX\_PG}{x^2} \cdot \frac{1}{(1.684 \cdot x)^2}$

Clearly, for a MAX_PG value and an "x" greater than or equal to one unit, and any value of $\angle BEA$ on the interval $(0, \pi/3)$

$$pseu\_g_A^F < pseu\_g_B^F.$$

Thus, the message from a node on the straight-line path, i.e., node A, does not necessarily result in the highest $pseu\_g$ value for node F. It is observed that the node with a higher total RSS product, i.e., node B, results in the higher $pseu\_g$ value. This is an important result for the proposed scheme. It is observed that the path resulting in the highest total RSS product to the *target node* is preferred over the path with the shortest distance. This implies that, although the chosen path of the AMR may be suboptimal in terms of distance, without any prior knowledge of the environment, this choice is preferable, since it indicates a clearer path between nodes with fewer obstructions and lesser interfering entities.

IV. WSN-ASSISTED NAVIGATION SCHEME

For AMRs, target-directed navigation is a standard motion planning problem. The key difference here is that the motion space is discretized by the locations of the WSN nodes. The node density of the WSN dictates how closely the motion space can be approximated by this discretization. The advantage is that the AMR does not concern itself with the nonrepresented space between two neighboring nodes, because it moves in straight-line paths between them.

Algorithm 2 shows the process followed by the AMR in navigating toward the *target node*.

Algorithm 2 PG-Following Navigation

1: **repeat**
2: Locate close to a node "n" (*guide* node) using RSS
3: **for all** neighbors "i" of node "n" **do** Get $pseu\_g$;
4: $\delta_n^i = pseu\_g_i - pseu\_g_n$;
5: **end for**
6: $\delta_n = \max_{\forall i} (\delta_n^i)$ ▷ if all $\delta_n^i < 0$, "n" is *target node*
7: nextNode = 'i^{th}' neighbor corresponding to δ_n;
8: Move to nextNode as node "n"
9: **until** "n" is *target node*, i.e.,. target is reached

The AMR discovers the "nextNode" by communicating in the neighborhood of the *guide* node. Once this is determined, the AMR interacts with this node (*guide* node) alone, in order to navigate toward it. By using the directional antennas and RSS, the bearing of a signal is estimated. The particular directional

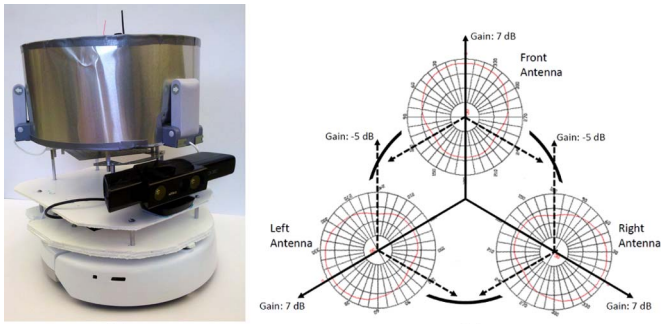

(a) (b)

Fig. 3. AMR platform and directional antenna radiation. (a) AMR platform. (b) Antenna radiation pattern on AMR.

antennas used for experimentation in this research are shown in Fig. 3(a) [18]. Its wireless radiation pattern [Fig. 3(b)] indicates a gain of 7 dBi in 0° [18]. Based on the radiation pattern, a 120° offset positioning of three-directional antennas maximizes the coverage around the AMR while minimizing the overlap of the radiation patterns. The AMR platform used for the experiments is shown in Fig. 3(a).

A weighted triangulation mechanism is used to estimate the bearing of the incoming wireless signal. Based on the RSS values at each directional antenna, two antennas with the higher values are chosen. Algorithm 3 shows the bearing estimation example for the "front" and "left" antennas being the antennas with the higher RSS values. The algorithm biases the bearing toward one antenna more than the other, based on the actual RSS values at the antennas. The *turnThreshold* parameter, used to determine this biasing, depends on the directional antenna gains and the maximum possible difference in the RSS values at the antennas.

The AMR, commanded to turn the computed bearing, then moves a predetermined distance in that direction. This bearing estimation and predetermined move sequence is continually repeated as the AMR incrementally moves toward the *guide* node. Once the RSS of the *guide* node at the AMR reaches a predetermined threshold, it is assumed that the *guide* node has been reached. The AMR is then commanded to repeat Algorithm 2 for the next *guide* node, and the navigation sequence begins again.

Algorithm 3 RSS Bearing Estimation (in degrees)

1: $\text{biasR} = 0.5 + (0.5 \cdot [Left - Front/turnThreshold])$;
2: $\text{biasL} = 1 - \text{biasR}$;
3: $\text{turnFactor} = [(\text{biasR} \cdot \text{Left} - \text{biasL} \cdot \text{Front})/\ (\text{biasR} \cdot \text{Left} + \text{biasL} \cdot \text{Front})]$;
4: $\text{Bearing} = \text{turnFactor} \cdot 60 + 60$;

V. EXPERIMENTAL ANALYSIS

Two critical requirements with respect to WSN-assisted AMR navigation act as performance bounds for the system.

1) There needs to exist a geographic path from any starting point for the AMR to traverse and reach the target.

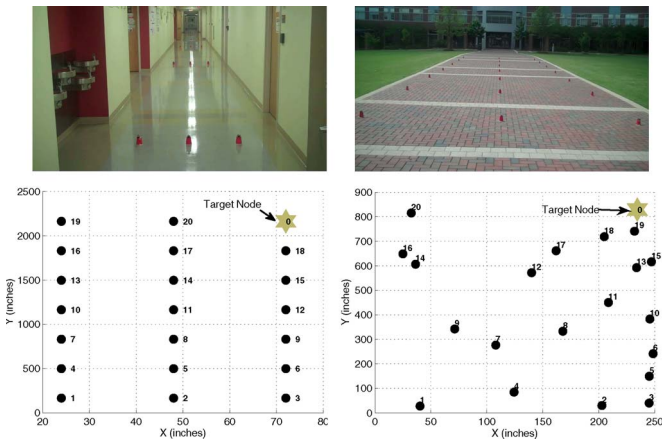

Fig. 4. Hardware setup for PG algorithm (indoor and outdoor).

TABLE II
PARAMETERS FOR HARDWARE TESTING

Parameter	Value	Parameter	Value
Tx Power	-25 dBm	Area (Outdoor)	256″ x 873″
Area (Indoor)	96″ x 2328″	AMR travel / step	0.3048 m (1 ft.)

The environment considered in our experiments is with or without obstacles. The physical region and obstacle placement need to be such that the target is not completely occluded from the AMR in terms of path traversal.

2) If a geographic path exists, then the WSN deployment shall be such that there exist nodes physically located on or close to that path. The proximity of the nodes to this path, a necessary condition for the algorithm to be useful, depends on how narrow or broad the allowable trajectory for the AMR is.

The implementation of the PG algorithm is tested in simulation and hardware (indoor and outdoor). The simulations were conducted with 30 different random generations of node locations, and a 95% confidence interval is computed for the data. For the simulation data, the *Free-Space* and *Log-Normal shadowing* (hereinafter, referred simply as Shadowing) path-loss models [10] are used. For the *Free-Space* model, the gains and the loss factor are assumed unity. Based on empirical tables for the *Shadowing* model [10], the path-loss exponent (β) for the indoor setting is chosen to be 1.5, while for the outdoor setting, it is two. The sigma (σ_{dB}) for both cases is assumed to be five. For communication, the TMote Sky nodes implement a basic low-level Carrier Sense Multiple Access protocol, which is also adopted for the simulations. Since traditional flooding is used, time synchronization of the nodes is not necessary.

Fig. 4 shows a photograph of the indoor and outdoor test beds for the hardware experimentation. Table II gives the parameters used for the hardware implementation. The algorithm was tested in a 21-node network. One *grid* layout of 7×3 nodes and three different *random* layouts (in the same area, with the same overall dimensions as the *grid* layout) were implemented. The random locations were drawn from a uniform distribution over the interval defined by the area dimensions. In each scenario, node ID "0" was assigned to be the *target node*. MAX_PG was set to 1000, and MAX_HC was set to 250. The maximum receiver sensitivity was kept at -95 dBm, and the minimum was kept at -5 dBm, based on the TMote Sky datasheet [16]. For each layout in the indoor and outdoor settings, the data presented are averaged over three experimental runs, giving a total of 12 experiments. The grid layout data are themselves averaged over two experiments, by exchanging nodes "0" and "1" to overcome any location bias.

The following performance metrics are used for the analysis.

1) Correlation coefficient: It gives insight into the simulated and real-world performances; its value defines the quality of the linear relationship between the data obtained in the scenarios.
2) Travel-distance ratio: It is the ratio of the actual distance traveled by the AMR to the Euclidean distance between its start location and the *target node*.
3) Number of nodes in trajectory: It is the number of *guide* nodes in the AMR trajectory from its start location to the *target node*.
4) Area of trajectory: It is the area under the curve of the trajectory from the AMR start location to the *target node*, bounded by the straight line connecting the two locations.
5) Bearing estimation: It displays the relationship between the actual bearing and the estimated bearing for the AMR as calculated using Algorithm 3.

A. Network Experiments

For the PG algorithm, comparing the magnitude distributions in simulation and hardware (Fig. 5), it is observed that the values follow the same trend of peaks and troughs based on the node locations, although the absolute values show variation. It is also observed that nodes at same hop-count level and/or the same physical distance away from the target node tend to show up at different distances. Although an artifact of the shadowing and interference effects on radio propagation, this property is advantageous since it indicates quality of link between nodes at particular locations. The variation is also attributed to the orientation of the sensor nodes on the ground, which, in turn, affects the signal strength in different directions. The TMote Sky nodes have an onboard inverted-F antenna [16] that has a nonideal radiation pattern.

For the correlation coefficient, the variables are the 21-element $pseu\_g$-value vectors, one each for the hardware experiment, the Free-Space simulation, and the Shadowing model simulation data. Fig. 6 demonstrates the correlation coefficients for the "Free-Space Model-to-Hardware" and the "Shadowing Model-to-Hardware" data relationships, for the indoor and outdoor test beds. Evidently, the choice of the path-loss model plays a critical role in the accuracy of the simulation experiments vis-à-vis the hardware experiments. The correlation coefficients demonstrate good-to-strong correlation between the RSS values in the real world and the simulated world. As expected though, the Shadowing model shows only good correlation, where the data for outdoor scenarios show even lower correlation. This is attributed to lack of good approximation for the Shadowing model parameters and environmental

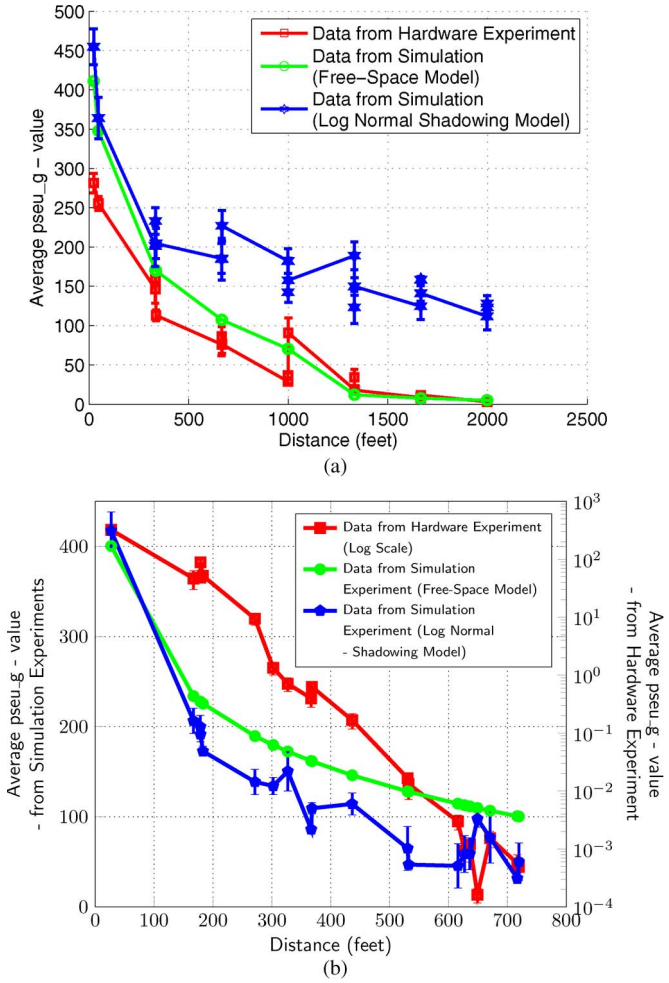

Fig. 5. *pseu_g*-value comparison—simulation and hardware (example data). (a) Grid layout (indoor). (b) Random layout (outdoor).

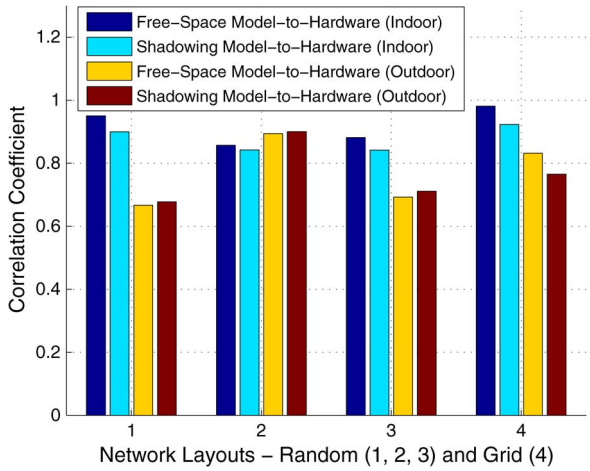

Fig. 6. Comparison of correlation coefficients comparing simulation and hardware performance.

variation. It is noted that humidity and temperature in outdoor environments also impact the values.

B. AMR Navigation Effectiveness

To analyze the effectiveness of the algorithm, the PG algorithm was compared to mechanisms proposed in [12] (FNF scheme), [14] (LiRosaRus scheme), and [19] (Reich scheme). Fig. 7 shows the difference in trajectories for the four methods from the same starting point to a target. Figs. 8 and 9 show the

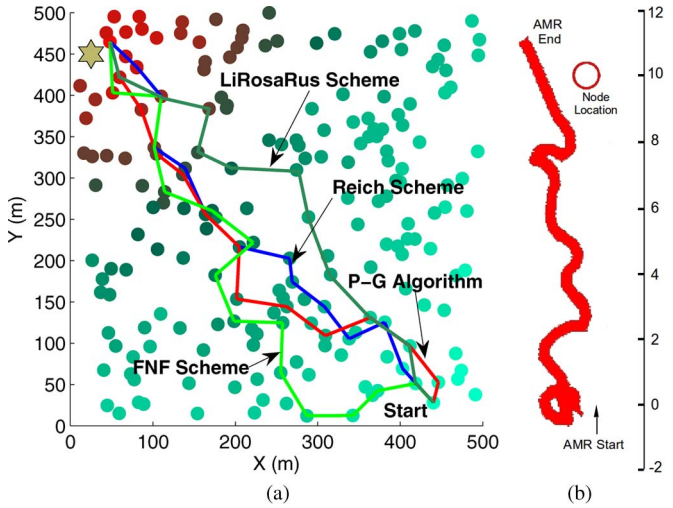

Fig. 7. AMR trajectories. (a) Trajectories for the four schemes. (b) AMR trajectory (in feet) for single-node navigation using Algorithms 2 and 3.

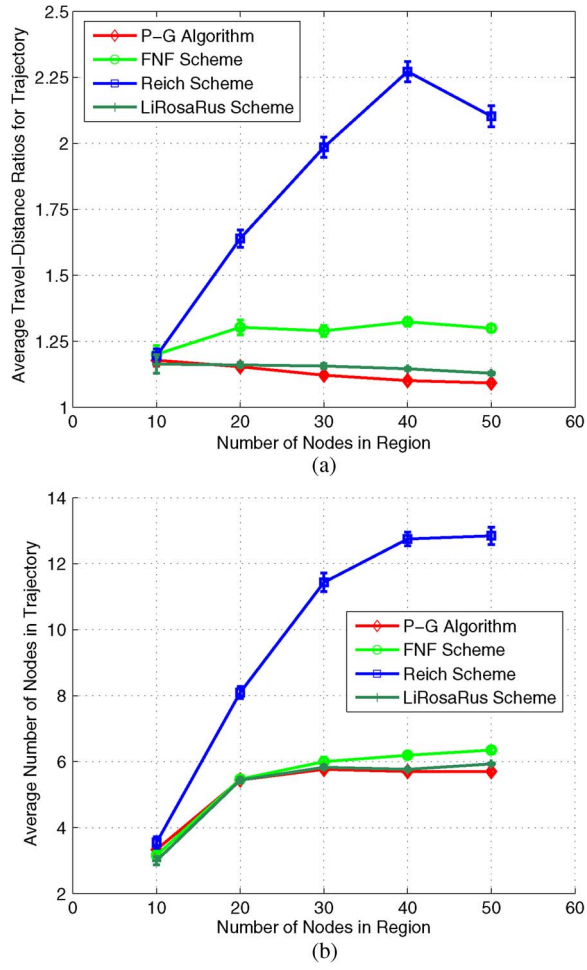

Fig. 8. Trajectory comparison for PG algorithm. (a) Travel-distance ratios [region area—300 × 300 m^2]. (b) Number of nodes in trajectory [region area—300 × 300 m^2].

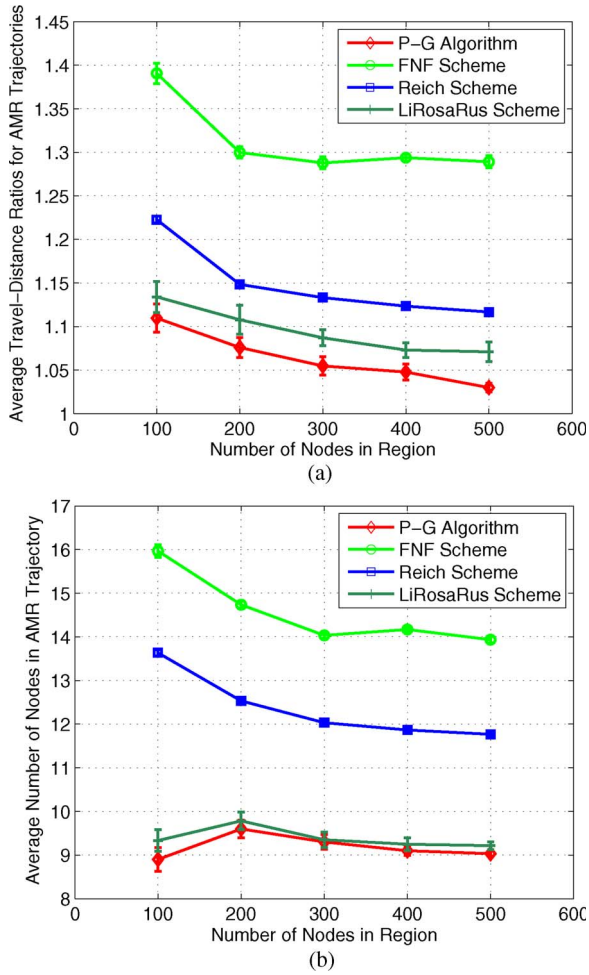

Fig. 9. Trajectory comparison for PG algorithm. (a) Travel-distance ratios [region area—650×650 m^2]. (b) Number of nodes in trajectory [region area—650×650 m^2].

travel-distance ratio and number-of-nodes parameter. Two key observations are made from the figures.

1) As seen, the PG algorithm performs better than all the other comparable schemes. Since RSS is used to scale the magnitude in a neighborhood, the effect is to create a steeper gradient in the neighborhood [see Fig. 1(b)], which leads to a shorter path for the AMR to follow.
2) The trends depend on the number of nodes in the region. It was observed that, for lower numbers (10–50), the region is not covered optimally, implying that the AMR has to travel longer distances between nodes. It also requires to use more *guide* nodes since the region is sparsely covered. As the node count increases, the coverage improves, thereby reducing the travel distance and the number of required *guide* nodes.

This simulation performance of the navigation scheme is then compared with that of the 21-node hardware implementation. The signal variations in the physical experiments have a significant impact on the AMR trajectory. The hardware layouts were also simulated with the Free-Space and Shadowing models to obtain simulated trajectories to compare with the actual AMR ones. Fig. 10 shows a comparison of trajectories that the AMR would take in moving from a starting node to the *target node* (shown as node "0"). It is immediately seen that the hardware experiments perform worse than the simulation experiments. The data for Tables III and IV summarize the related performance metrics.

The following observations can be drawn from the tables.

1) It was observed that the communication ranges for the nodes in simulation were higher than the range that the hardware nodes experienced, for the same transmission power. Due to this, the simulation experiments allowed at most a one-hop or two-hop communication between the *target node* and all other nodes in the network. In contrast, the hop counts during the hardware experimentation were much higher. This impacted the trajectories for the respective methods. This is also expected following from the correlation data in Fig. 6.
2) The grid layout experiments perform better than the random layouts. This is expected since the grid layout allows uniform and regular coverage of the region, reducing the travel distance and communication overhead for the AMR.
3) The numbers for indoor experiments are much lower than those for outdoor experiments. In addition to the multipath fading, interference, and environmental variations, this is also attributed to the *waveguide* effect [22]. The walls of the corridor confine more electromagnetic waves along its length, assisting the propagation of the wave further than in the outdoor case, causing more nodes to receive the target-node message in the first hop itself. This reduced the trajectories for the indoor layouts.
4) For the indoor experiments, the Shadowing model experiments perform the best, while for the outdoors, it is the Free-Space model experiments that outperform the others. This again follows from Fig. 6. The model parameters in the indoor scenario are more stable than those in the outdoor environment.

It is evident from the tables that, the higher the number of nodes in the trajectory, the greater are the trajectory area and the travel-distance ratio. In observing the data, the indoor data show more variations in the metric values over the layouts than the outdoor data. This is again an artifact of multipath effects and signal interference.

The bearing estimation algorithm for the directional antennas of the AMR was tested using a stationary wireless transmitter node at three distances—5, 15, and 25 ft. For each distance, the AMR was rotated in place counterclockwise, in steps of 30°, for the full 360°. Then, based on the algorithm, the output bearing for the AMR was determined.[3] Fig. 11(a) is a glimpse of the variation in RSS value variation at the three antennas—here, for 5-ft distance in outdoor setting. The readings follow the overall expected trend of crests and troughs for counterclockwise rotation of the AMR.[4] Generally, for the indoor and outdoor

[3]Zero degree is with the front antenna of AMR pointing in the direction of the stationary transmitter.

[4]Antenna (crest, trough): Front (0°, 180°), Left (120°, −60°), Right (−120°, 60°).

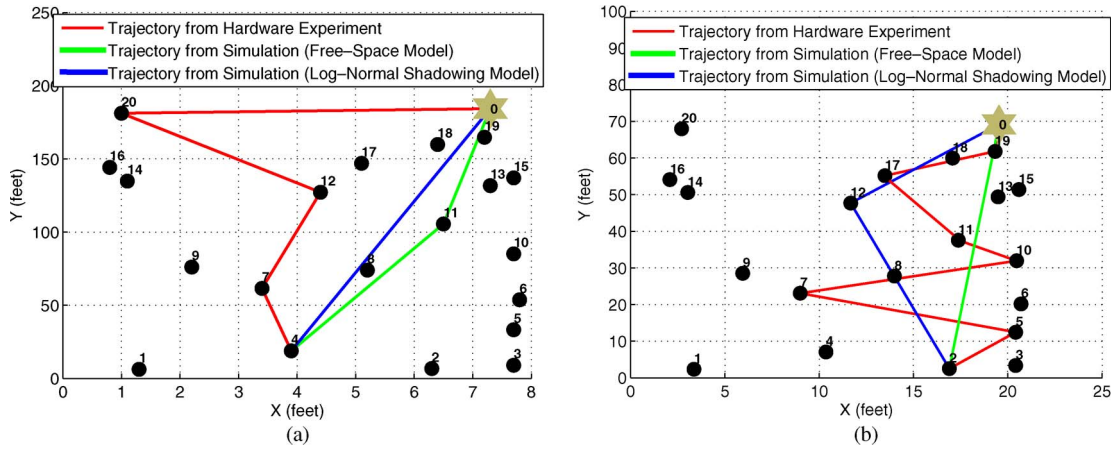

Fig. 10. Trajectory comparison with hardware experiments. (a) Indoor. (b) Outdoor.

TABLE III
TRAJECTORY PARAMETERS (INDOOR)

		Area of Trajectory (ft^2)			Travel-Distance Ratios			Traj. Number of Nodes		
		Hardware	Free-Space	Shadowing	Hardware	Free-Space	Shadowing	Hardware	Free-Space	Shadowing
Grid Layout		214.7	322.1	73.4	1.012	1.000	1.000	4	3	2
Random	Layout 1	1810.0	153.3	85.6	1.024	1.000	1.000	5	3	2
	Layout 2	82.08	90.13	57.3	1.000	1.000	1.000	3	3	2
	Layout 3	6671.0	4276.0	584.2	1.008	1.000	1.000	4	4	2

TABLE IV
TRAJECTORY PARAMETERS (OUTDOOR)

		Area of Trajectory (ft^2)			Travel-Distance Ratios			Traj. Number of Nodes		
		Hardware	Free-Space	Shadowing	Hardware	Free-Space	Shadowing	Hardware	Free-Space	Shadowing
Grid Layout		1.022	0	0	1.202	1.000	1.000	5	2	2
Random	Layout 1	5839.0	203.1	635.4	1.706	1.000	1.025	7	3	2
	Layout 2	85.63	23.1	46.95	1.541	1.000	1.120	6	3	2
	Layout 3	1793.0	56.0	139.4	1.369	1.000	1.012	6	3	2

experiments, similar trends were observed, with more noise in the outdoor experiment data, as expected. It was observed that, as the distance increases, the absolute values reduce.

Based on [18], the directional antenna has a gain of 7 dBi in its zero heading. As can be seen in Fig. 3(b), if the incoming signal is directly in line with the "Front" antenna, then the ideal gain of the signal received at the "Front" antenna will be 7 dB over that for a colocated omnidirectional antenna. At the same time, the "Left" and "Right" antennas will show a negative gain of 5 dB, since the signal is recorded at -120° and 120° angles from the zero heading. Therefore, the theoretical *turnThreshold* for the setup will be $7-(-5)=12$ dB. Fig. 11(b) shows the error in bearing estimate calculated using this *turnThreshold* value. As is seen, the error is significant, and the outdoor data show a higher error in the bearing estimate. It is also observed that, for indoor environments, the closer node is resolved better than the farther node, while the converse is true for the outdoor environments. Fig. 7(b) shows an example trajectory for the AMR (indoors) using Algorithms 2 and 3, with the node located 10 ft away. A combination of factors, including the overlap of the radiation patterns of the antennas, the proximity of the antennas to each other on the AMR body, and variations in the RF signal propagation, is responsible for the nonoptimal trajectory. Further experimentation in this context can help determine a dynamic *turnThreshold*, which will weigh the three antenna readings proportionally.

VI. CONCLUSION AND FUTURE WORK

In this paper, a novel mechanism for localizing targets in unknown environments using a static WSN has been demonstrated. The important feature of the technique is that it does not rely on global positioning information and utilizes only RSS to navigate the AMR. This fact allows the "PG" algorithm to operate inside buildings or forested areas, without having to resort to any sophisticated hardware like GPS. The utility of the algorithm is successfully demonstrated via simulation and hardware implementations. This paper has introduced five metrics for performance analysis, and the PG algorithm has shown better performance in comparison to other existing schemes.

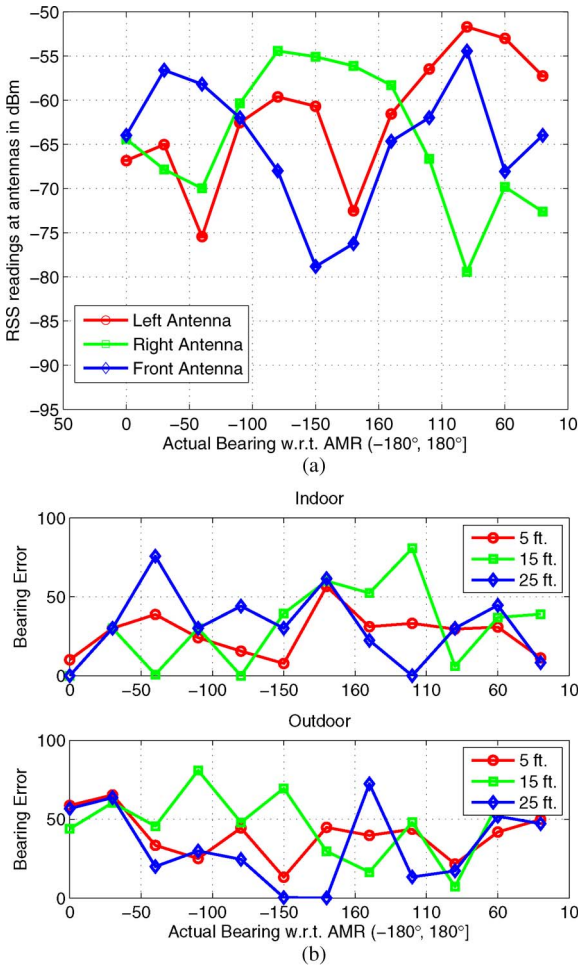

Fig. 11. Directional antenna experiments. (a) RSS values at 5 ft (outdoor). (b) Bearing estimation error (in degrees).

Notably, the metrics also help understand the quality of results obtained in simulation and hardware. The metrics bear out the communication burden of the sensor nodes, the travel time and distance for navigation to a target, and the utility of the RF path-loss modeling for the environment. The low computational complexity of the PG algorithm allows it to be robust enough to be applied in real-world applications. As expected, hardware experiments perform worse than the simulation experiments, and this aspect needs further investigation.

For future research, three aspects that shall be explored extensively include the following: 1) performance degradation in harsh environments with obstacles, as well as node and link failures; 2) coordinated multiple AMR navigation; and 3) probabilistic way-point-based navigation. It is clear from the data on the bearing estimation that more intelligent strategies are required to be adopted. Probabilistic filtering of the bearings will account for the uncertainties in the RSS–distance relationship and the antenna radiation patterns. Early experiments of such a scheme have shown promising results, giving much smoother shorter trajectories, allowing for coordinated motion of multiple AMRs. Further hardware experimentation is needed to ascertain the level of accuracy and robustness of the mechanism using real-time WSN–AMR coordination. The research continues.

REFERENCES

[1] I. F. Akyildiz, W. Su, Y. Sankarasubramaniam, and E. Cayirci, "Wireless sensor networks: A survey," *Comput. Netw.*, vol. 38, no. 4, pp. 393–422, Mar. 2002.

[2] A. Arora, P. Dutta, S. Bapat, V. Kulathumani, H. Zhang, V. Naik, V. Mittal, H. Cao, M. Demirbas, M. Gouda, Y. Choi, T. Herman, S. Kulkarni, U. Arumugam, M. Nesterenko, A. Vora, and M. Miyashita, "A line in the sand: A wireless sensor network for target detection, classification and tracking," *Comput. Netw.*, vol. 46, no. 5, pp. 605–634, Dec. 2004, Military Communications Systems and Technologies.

[3] J. Bachrach, R. Nagpal, M. Salib, and H. Shrobe, "Experimental results for and theoretical analysis of a self-organizing global coordinate system for ad hoc sensor networks," *Telecommun. Syst.*, vol. 26, no. 2–4, pp. 213–233, Jun. 2004.

[4] M. A. Batalin and G. S. Sukhatme, "Sensor network-mediated multi-robot task allocation," in *Proc. 3rd Intl. Naval Res. Lab. Multi-Robot Syst. Workshop*, Mar. 2005, pp. 27–38.

[5] M. A. Batalin, G. S. Sukhatme, and M. Hattig, "Mobile robot navigation using a sensor network," in *Proc. IEEE ICRA*, 2004, pp. 636–641.

[6] J. Blumenthal, F. Reichenbach, and D. Timmermann, "Minimal transmission power vs. signal strength as distance estimation for localization in wireless sensor networks," in *Proc. 3rd Annu. IEEE Commun. Soc. Sens. Ad Hoc Commun. Netw.*, 2006, pp. 761–766.

[7] Y. Chen and T. C. Henderson, "S-NETS: Smart sensor networks," in *Proc. ISER*, Dec. 2000, pp. 81–90.

[8] P. Corke, R. Peterson, and D. Rus, "Localization and navigation assisted by networked cooperating sensors and robots," *Int. J. Robot. Res.*, vol. 24, no. 9, pp. 771–786, Sep. 2005.

[9] N. Deshpande, E. Grant, and T. C. Henderson, "Experiments with a "pseudo-gradient" algorithm for target localization using wireless sensor networks," in *Proc. IEEE Int. Conf. MFI*, Sep. 2010, pp. 74–79.

[10] A. Goldsmith, *Wireless Communications*. Cambridge, U.K.: Cambridge Univ. Press, 2005.

[11] T. C. Henderson and E. Grant, "Gradient calculation in sensor networks," in *Proc. IEEE/RSJ Int. Conf. IROS*, Sep./Oct. 2004, pp. 1792–1795.

[12] J.-R. Jiang, Y.-L. Lai, and F.-C. Deng, "Mobile robot coordination and navigation with directional antennas in positionless wireless sensor networks," in *Proc. Int. Conf. Mobility*, 2008, pp. 1–7.

[13] K. Kotay, R. Peterson, and D. Rus, "Experiments with robots and sensor networks for mapping and navigation," in *Proc. Int. Conf. Field Service Robot.*, vol. 25, *ser. STAR*, P. Corke and S. Sukkarieh, Eds., Jul. 2005, pp. 243–254.

[14] Q. Li, M. De Rosa, and D. Rus, "Distributed algorithms for guiding navigation across a sensor network," in *Proc. 9th Int. Conf. MobiCom*, 2003, pp. 313–325.

[15] K. A. Luthy, E. Grant, and T. C. Henderson, "Leveraging RSSI for robotic repair of disconnected wireless sensor networks," in *Proc. IEEE ICRA*, Apr. 2007, pp. 3659–3664.

[16] MOTEIV Corporation (now Sentilla), Accessed on 7 March 2012, Moteiv TMote Sky Datasheet 2007. [Online]. Available: http://www.snm.ethz.ch/Projects/TmoteSky

[17] N. Potnis, A. Mahajan, K. Gopalan, and A. Wang, "Evaluation of mesh-enhanced VANET deployment models," in *Proc. 16th ICCCN*, Aug. 2007, pp. 862–867.

[18] DPAC Technologies. ACH2-AT-DP006 Directional Antenna 2003. [Online]. Available: http://www.quatech.com/catalog/accessories.php

[19] J. Reich and E. Sklar, "Robot-sensor networks for search and rescue," in *Proc. IEEE Int. Workshop Safety, Secur. Rescue Robot.*, 2006.

[20] R. Severino and M. Alves, "Engineering a search and rescue application with a wireless sensor network-based localization mechanism," in *Proc. IEEE Int. Symp. WoWMoM*, 2007, pp. 1–4.

[21] J.-P. Sheu, K.-Y. Hsieh, and P.-W. Cheng, "Design and implementation of mobile robot for nodes replacement in wireless sensor networks," *J. Inf. Sci. Eng.*, vol. 24, no. 2, pp. 393–410, Mar. 2008.

[22] M. L. Stowell, B. J. Fasenfest, and D. A. White, "Investigation of radar propagation in buildings: A 10-billion element Cartesian-mesh FETD simulation," *IEEE Trans. Antennas Propag.*, vol. 56, no. 8, pp. 2241–2250, Aug. 2008.

[23] A. S. Tanenbaum, *Computer Networks*. Englewood Cliffs, NJ, USA: Prentice-Hall PTR, 2002.

[24] A. Verma, H. Sawant, and J. Tan, "Selection and navigation of mobile sensor nodes using a sensor network," in *Proc. 3rd IEEE Int. Conf. PerCom*, 2005, pp. 41–50.

[25] S. Yang and H. Cha, "An empirical study of antenna characteristics toward RF-based localization for IEEE 802.15.4 sensor nodes," in *Proc. 4th EWSN*, vol. 4373, *LNCS*, K. Langendoen and T. Voigt, Eds., 2007, pp. 309–324.

[26] B. Zhang and G. S. Sukhatme, "Controlling sensor density using mobility," in *Proc. 2nd IEEE Workshop EmNetS-II*, 2005, pp. 141–150.

Nikhil Deshpande (S'03) received the B.Eng. degree in electrical engineering from the Government College of Engineering, University of Pune, Pune, India, in 2003 and the M.S. degree in integrated manufacturing systems engineering from North Carolina State University, Raleigh, NC, USA, in 2007, where he is currently working toward the Ph.D. degree in the Department of Electrical and Computer Engineering.

His general interests are in the areas of autonomous robotics and wireless sensor networks. More specifically, he is studying the effectiveness of autonomous navigation through intelligent interaction with wireless sensor networks.

Edward Grant (M'89–SM'00) received the B.Sc.(Hons.) degree in mechanical engineering from the University of Abertay Dundee, Dundee, U.K., the M.Eng. degree in fluid power control from the University of Sheffield, Sheffield, U.K., and the Ph.D. degree in computer science from the University of Strathclyde, Glasgow, U.K.

He is currently a Professor of electrical and computer engineering and biomedical engineering with North Carolina State University, Raleigh, NC, USA, where he is the Director of the Center for Robotics and Intelligent Machines. Since 2010, he has an appointment as a Senior Researcher with the Italian Institute of Technology. His research interests include evolutionary robotics, medical robotics, and smart wearable sensing and control systems for health care.

Prof. Grant is a Chartered Engineer and a fellow of the Institution of Mechanical Engineers.

Thomas C. Henderson (M'82–SM'96–F'03) received the B.S. degree in math (with honors) from Louisiana State University, Baton Rouge, LA, USA, in 1973 and the Ph.D. degree in computer science from the University of Texas, Austin, TX, USA, in 1979.

He was a Visiting Professor at the German Aerospace Center (DLR), Oberpfaffenhofen, Germany, in 1980, the Institut National de Recherche en Informatique et en Automatique, Paris, France, in 1981 and 1987, and the University of Karlsruhe, Karlsruhe, Germany, in 2003. Since 1982, he has been with the School of Computing, University of Utah, Salt Lake City, UT, USA, where he was the Chairman of the Department of Computer Science in 1991–1997, was the Founding Director of the School of Computing in 2000–2003, and is currently a Professor. Producing over 200 scholarly publications, he has been the Principal Investigator on over $8 M in research funding. He is the author of *Discrete Relaxation Techniques* (Oxford University Press), is an Editor of *Traditional and Non-Traditional Robotic Sensors* (Springer-Verlag), and served as Co-Editor-in-Chief of *Robotics and Autonomous Systems Journal*. His research interests include autonomous agents, robotics, and computer vision, and his ultimate goal is to help realize functional androids.

Prof. Henderson was the recipient of the Governor's Medal for Science and Technology in 2000. He was an Associate Editor for the IEEE TRANSACTIONS ON PATTERN ANALYSIS AND MACHINE INTELLIGENCE and IEEE TRANSACTIONS ON ROBOTICS AND AUTOMATION.